High-pressure Raman study of microcrystalline WO_3 tungsten oxide

2002 J. Phys.: Condens. Matter 14 5849

(http://iopscience.iop.org/0953-8984/14/23/314)

INSTITUTE OF PHYSICS PUBLISHING JOURNAL OF PHYSICS: CONDENSED MATTER

J. Phys.: Condens. Matter **14** (2002) 5849–5863 PII: S0953-8984(02)31332-8

High-pressure Raman study of microcrystalline WO_3 tungsten oxide

M Boulova[1,2], N Rosman[1], P Bouvier[1] and G Lucazeau[1,3]

[1] Laboratoire d'Electrochimie et de Physico-Chimie des Matériaux et des Interfaces (CNRS UMR 5631), ENSEEG-INPG, 1130 rue de la Piscine, BP75, 38402 St Martin d'Hères Cedex, France
[2] Chemistry Department, Moscow State University, Moscow, 119899, Russia

Received 28 November 2001, in final form 8 May 2002
Published 30 May 2002
Online at stacks.iop.org/JPhysCM/14/5849

Abstract

A high-pressure Raman study of microcrystalline tungsten oxide was performed in the 0.1 MPa–30 GPa pressure range under hydrostatic and non-hydrostatic conditions. Two phase transitions are evidenced; they take place below 0.1 GPa and at about 22 GPa and are of first order. Two spectral anomalies are observed at about 3 and 10 GPa; they may be related to diffuse weak structural transitions. The number of observed Raman bands remains practically unchanged in the 0.1–30 GPa range and thus the symmetry changes are likely to be small. Surprisingly, the non-hydrostatic conditions do not induce inhomogeneous band broadening and do not modify the transition sequence observed in hydrostatic conditions. The compressibilities of the different observed phases are estimated from spectral data and discussed within Hazen's polyhedral approach.

1. Introduction

Tungsten trioxide, WO_3, is the focus of an intensive research effort because of its great applicability in electrochromic devices, catalysis, and as a precursor for hard-material synthesis, etc. Recently, nanocrystalline oxides such as tin oxide, zirconia, and tungsten oxide were used in gas sensors; this has stimulated studies of the effect of the nanometric size of crystallites on the P–T phase diagram and on the chemical reactivity of such oxides [1–4].

The structure of this compound can be described as deriving from an ABO_3 perovskite structure in which the A cation is missing. As a function of temperature, WO_3 gives rise to a large variety of phases [5] which, in addition, exhibit a broad metastability domain. In this respect, depending on the crystallite size, or the film or bulk state, different phases may result from the same thermal and pressure treatment. Although the triclinic δ-form (space group $P\bar{1}$, $Z = 8$) is considered to be thermodynamically stable at room temperature, it coexists with a number of other phases such as the monoclinic γ-form ($P2_1/n$, $Z = 8$) and also possibly with the low-temperature monoclinic ε-form (Pc, $Z = 4$) [6–10].

[3] Author to whom any correspondence should be addressed.

Table 1. Structural data as reported in the literature.

Reference [12]		Reference [13]		
Phase	Transition temperature (K)	Phase	Transition temperature (K)	Structural notation
$P4/nmm$	1170	$P4/ncc$	1073	α
$P4/ncc$	1000			
$P\bar{4}2_1m$				
$Cmca$	600	$Pbcn$	623	β
$Pnma$				
$P2_1/n$				γ
$P\bar{1}$	230			δ
Pc				ϵ

Literature data on high-pressure (HP) investigations of tungsten trioxide phase transitions are scarce. In their early HP study of WO_3, Salje and Hoppmann [11] observed that the initial sample was a mixture of γ- and δ-phases. Under modest pressure the monoclinic γ-phase partially transforms, first to a triclinic δ-phase at 0.1 GPa, and then, on further pressure increase, completely to the ε-phase at 0.155 GPa. On the other hand, from a x-ray diffraction (XRD) study of a WO_3 single crystal up to 5.7 GPa, Xu *et al* [8] conclude that the triclinic form transforms into a $P2_1/c$ phase above 0.57 GPa, different from the ε-phase reported by Salje *et al*. Finally, from Raman investigations, Souza-Filho *et al* [12] conclude that the complete transformation of the initial mixture of phases takes place above 1.4 GPa and that the structure of this HP phase can be described by the Pc or $P2_1/c$ space group as suggested by the above XRD studies [8,11] without putting forward new spectroscopic arguments to enable a decision to be made about its structure. Table 1 gives an overview on the different temperature- and pressure-dependent phases reported in the literature; to the best of our knowledge, there are no data available for pressures above 5 GPa.

Recently, several crystal structures of WO_3 have been studied with the first-principles pseudopotential method [13]. The authors conclude that the electronic gap increases with the distortion of the octahedra and with the tilting of the octahedra upon compression. The crystal responds to pressure only by a rotation of the octahedra. The range of cell volumes investigated corresponds to 4.7 GPa, the highest pressure measured in [8].

The present work is part of a systematic study of physical properties of nanocrystallized and microcrystallized WO_3 and is the continuation of a preliminary study reporting on the comparison between the effects of pressure on nanocrystalline and microcrystalline tungsten oxide [2]. The present work is focused on the study of the effect of hydrostatic and non-hydrostatic pressure up to 30 GPa on microcrystalline WO_3.

2. Symmetry considerations and vibrational selection rules

The Raman spectra of ambient and low-temperature phases of WO_3 are expected to show a large number of vibrational bands. This complexity is due to a unit-cell multiplicity varying between four and eight and to a low symmetry for all the phases identified in the literature. This is amplified for the initial powder that is made of a mixture of monoclinic and triclinic phases.

The structure of the room-temperature monoclinic phase γ is described by the $P2_1/n$ space group with $Z = 8$ and can be viewed as made of corner-linked distorted WO_6 octahedra, just as in perovskites. After subtraction of the A_u and B_u acoustic modes, the vibrational modes are

distributed among the following irreducible representations: $\Gamma_{opt} = 24A_g+24B_g+23A_u+22B_u$, among which the $24A_g$ and $24B_g$ modes are Raman active.

For the triclinic δ-phase ($P1$, $Z = 8$), 45 infrared-active modes of A_u symmetry and 48 Raman-active modes of A_g symmetry are expected.

24 Raman-active modes are expected for the two different HP structures proposed in the literature:

- The structure of the HP form reported in [8] is $P2_1/c$ with $Z = 4$ leading to: $\Gamma_{opt} = 12A_g + 12B_g + 11A_u + 10B_u$, where the 24 Raman-active modes are of A_g and B_g symmetry.
- Finally, for the ε-phase (Pc, $Z = 4$), the 45 optical modes ($23A''$ and $22A'$) are both Raman and infrared active.

3. Experimental procedure

The tungsten oxide powder, 99.995% pure, was obtained from Aldrich. The initial phase composition was deduced from XRD and the sample was found to be a mixture of monoclinic γ- and triclinic δ-structures in an approximate ratio of 90:10. The average size of the crystallites, determined by using the Scherrer formula [14], is found about 0.5 μm.

Raman spectra were obtained using a backscattering geometry on a XY Dilor multichannel spectrometer equipped with a CCD detector. The 514.53 nm line from an argon-ion laser was used as the excitation source. Powers of about 5 mW incident on the sample were used. The sample was placed in a membrane diamond anvil cell (DAC) from BETSA, where an Inconel gasket was used as the sample chamber. The pressure-transmitting medium was a 4:1 ethanol–methanol mixture. A second type of pressure investigation consisted in studying the powder without a transmitting medium, i.e. the gasket was filled completely with powder. In both types of experiment, small fragments of ruby were distributed all around the sample in order to obtain accurate measurements of the local pressure from the ruby fluorescence lines used as internal indicators of the applied pressure [15]. Gradients of 0.1–0.3 GPa were observed and can be considered as the order of the precision of the pressure values. Unfortunately, the DAC is not well adapted to the 10–200 MPa low-pressure range. In particular, it is impossible to perform an accurate measurement of the internal pressure below 0.1 GPa. Therefore, the corresponding pressure values reported in this work were estimated from a reference curve relating the values of the internal pressure to the primary external pressure.

After focusing with a $\times 20$-magnification microscope objective, the laser spot was about 2 μm in diameter. All the spectra were decomposed into Lorentzian components using Jandel's Peakfit software. The wavenumber accuracy is about 0.1 cm^{-1} in the low-pressure range and about 0.2 cm^{-1} above 20 GPa. The recording time for each spectrum was 20 s for the 0.1 MPa–20 GPa range, and 120 s above 20 GPa.

4. Results

An overview of the Raman spectra obtained under hydrostatic HP conditions at room temperature from room atmosphere to 31 GPa is shown in figures 1 and 2. The low-frequency region of the five first spectra recorded under hydrostatic and non-hydrostatic conditions is represented in figure 3. Figure 4 represents the pressure dependence of the wavenumbers for different bands, hereafter identified by a number. Distinct changes in the evolution of the wavenumbers with applied pressure allow one to distinguish five different pressure ranges marked as HP1–HP4 in figures 1 and 2 and discussed in terms of pressure-induced structural transitions in the

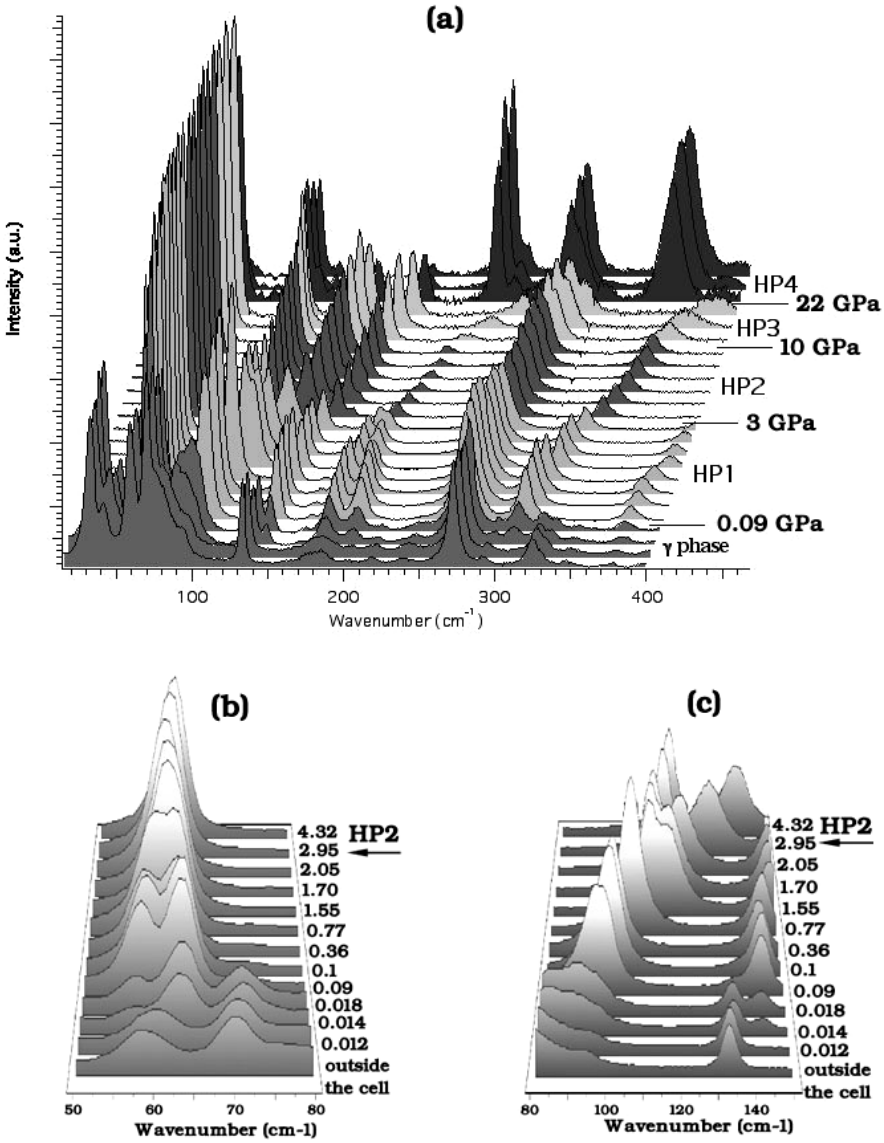

Figure 1. Raman spectra of WO_3 under isostatic pressure between 0.1 MPa and 31 GPa.

following. The identification of the pressure domains is somewhat imprecise and is based on the rapid changes in intensity, halfwidth, or wavenumbers observed in the spectra around the reported pressures. Figure 5 shows that the spectra obtained under non-hydrostatic conditions are made up of narrow bands and are close to those obtained under hydrostatic conditions.

4.1. Initial phases

The spectra for the 0.1 MPa–0.1 GPa pressure range appear characteristic of the initial mixture of phases. As underlined in the literature [11, 12], the initial microcrystalline sample consists of a mixture of monoclinic γ- and triclinic δ-phases, whose characteristic Raman bands are

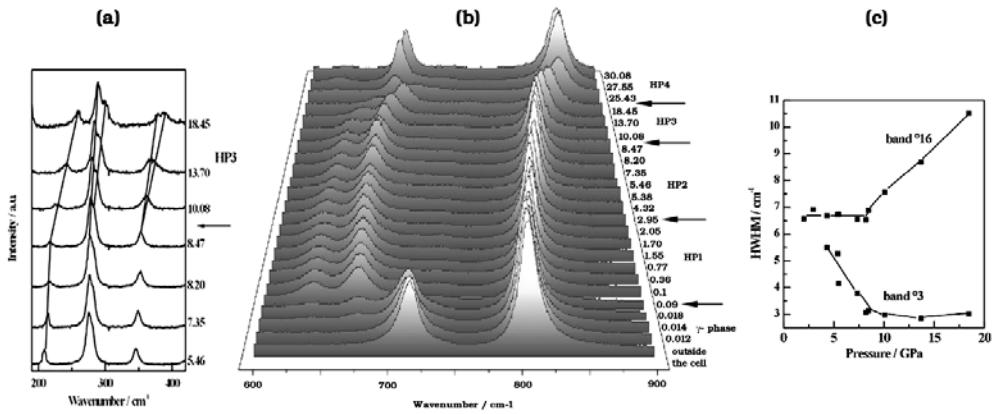

Figure 2. (a, b): Portions of Raman spectra of WO_3 under hydrostatic pressure, (c): Halfwidth of the bands #3 and 16 versus pressure under hydrostatic pressure conditions.

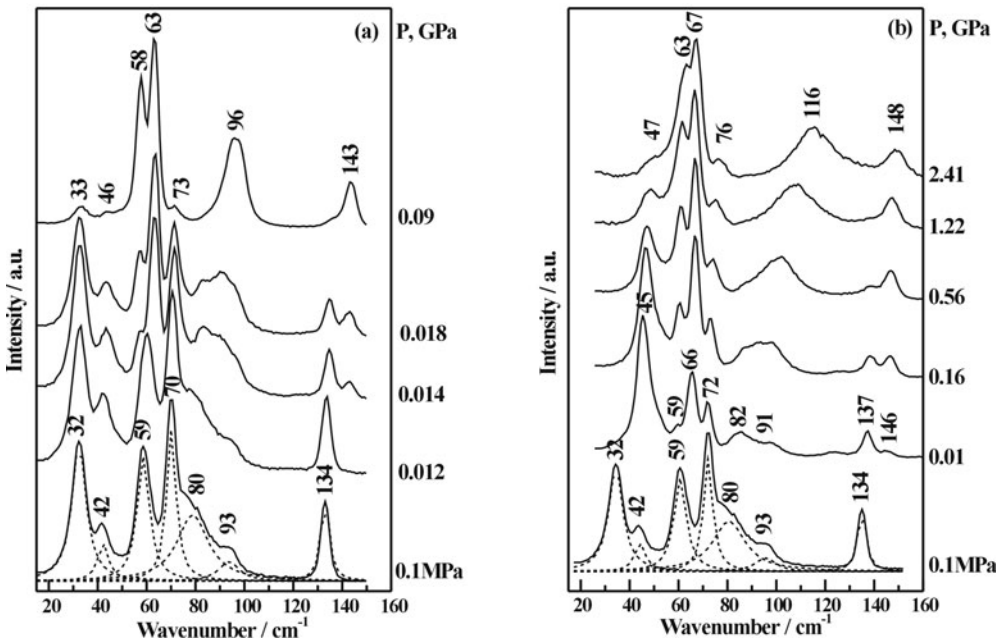

Figure 3. The low-frequency region of the Raman spectra under hydrostatic (a) and non-hydrostatic (b) low-pressure conditions.

the 32 and 42 cm^{-1} lines, respectively. In agreement with the x-ray results, the triclinic form contribution in the Raman spectrum is in the minority. When the sample is placed in alcohol and subjected to a small increment of pressure, the relative proportions of these phases do not change, but the growth of the band at 143 cm^{-1} is an indication that the HP1 phase begins to form. At 0.09 GPa (spectrum 5 in figure 3(a)) the transformation is complete. The same spectrum is obtained at 0.03 GPa in [12]. When the powder is placed between diamond anvils without transmitting fluid, as reported in [11], it already transforms into the stable triclinic phase (figure 3(b)) just under the weight of the anvils.

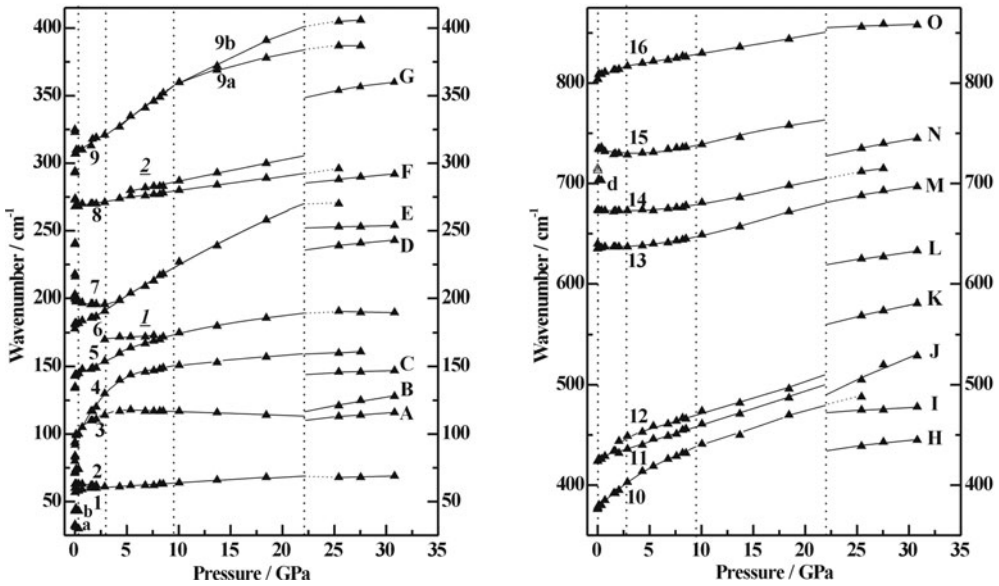

Figure 4. Pressure dependences of the wavenumbers of Raman bands. The solid curves are given as a guide to the eyes.

4.2. HP1 phase

The spectra observed in the 0.1–3 GPa pressure range can be considered as representative of the HP1 phase. The spectra are quite similar to those reported in [12]. The spectrum obtained at 0.36 GPa in alcohol is made up of at least 21 characteristic components, similar to that obtained at 0.28 GPa by Salje and Hoppmann [11]. Most of these features are still present at 2.05 GPa in alcohol or at 2.09 GPa without alcohol. Above this pressure some changes start to occur: the two components at about 60 cm^{-1} merge into a single band while the broad band at about 100 cm^{-1} splits into two components. It is worth mentioning that most of the low-frequency modes harden, while the reverse is true for high-frequency modes.

4.3. HP2 phase

The most spectacular change seen in noting the HP1/HP2 change is the sudden intensity decrease of the bands 6 and 7 (the doublet near 200 cm^{-1}) and their merging just below 3.5 GPa; this is seen in figure 1(a).

The splitting of the band at about 100 cm^{-1} into components 3 and 4 (figure 1(c)) is hardly observable at 1.55 GPa, it is equal to 15 cm^{-1} at 3 GPa, and reaches a plateau at 5 GPa (figure 4); the medium pressure (3 GPa) is chosen as the characteristic pressure associated with this evolution. The bands 1, 2 merge into a single component above 3 GPa (figure 1(b)). Above 3 GPa an important variation of the $\mathrm{d}\nu/\mathrm{d}p$ derivatives is observed for some modes: for instance, as shown in figure 4, the wavenumbers for bands 4 and 3, which were increasing rapidly with pressure in the HP1 phase, now reach a plateau, and even decrease for band 3. Above 5 GPa, that for band 7 ceases to decrease and merges with that for band 6, that for band 15 also ceases to decrease, and, more generally, all modes start to increase in wavenumber with pressure. New components, i.e. a new spectral signature, such as bands at 170 cm^{-1} (band ***1***), 432 cm^{-1} (band 11), and 444 cm^{-1} (band 12), start to appear above 2 GPa and are clearly separated at 3 GPa.

4.4. HP3 phase

Once more, in the 7–12 GPa pressure range, subtle changes suggest that a structural change might have taken place:

(i) the band ***1*** merges into band 5, and band 9 splits into two components: 9a and 9b; this is clearly observed in figures 1 and 2(a).

(ii) The splitting of the band 8 into two components is observed at about 10 GPa (figure 2(a)); in fact, a Lorentzian spectral decomposition indicates that this splitting (figure 4) seems to have started already below 7 GPa, and this indicates that the structural evolution takes place over a broad pressure range.

(iii) A certain number of curves in figure 4 undergo pronounced change of their derivatives—some even change the sign of their concavity around 10 GPa; this is the case for modes 4, 6, 9, 10. The halfwidth of band 16 increases much faster above 10 GPa. In contrast, band 3 gets narrower below 10 GPa and becomes steady at this pressure.

These changes are indications of instability of the crystal towards many degrees of freedom, and the fact that the $\nu = f(P)$ frequency plots do not follow an exponential or at least a linear law (see section 5.3.2) is an indication that important anharmonic processes are present in this pressure range. All these spectral changes are quite small and may correspond to weak isostructural changes (same space group, same site occupation, but sudden displacements of atoms in general positions). It is likely that these structural evolutions are so small that they cannot be detected by means of XRD under high pressure.

Notice that the choice of the pressure values 3 and 10 GPa to characterize the weak HP1/HP2 and HP2/HP3 transitions respectively results in an average of the pressure ranges in which anomalies are observed; these values are of course quite approximate in that the evolutions are spread over several GPa.

4.5. HP4 phase

A clear discontinuity in the evolution of spectra is observed between 18 and 25 GPa. It is interesting to note that some of the strong bands belonging to the HP3 phase can be detected beyond 25 and even 28 GPa, although their wavenumber does not undergo further change with pressure. Dotted horizontal lines in figure 4 correspond to remnant HP3 bands. The transition pressure of 22 GPa is obtained at the intersection of curves obtained by extrapolating the horizontal frequency plots of the HP4 phase with those of the HP3 phase.

Figure 5 allows us to compare Raman spectra of WO_3 under hydrostatic and non-hydrostatic conditions at about 14 and 30 GPa. One should note a spectacular reduction of the intensities of the bands of this phase, in particular for the non-hydrostatic conditions.

The wavenumbers of the bands resulting from a fitting procedure using Lorentzian components for pressures close to the those of four suspected transitions are reported in table 2; the corresponding $(\partial\nu/\partial P)_T$ coefficients are also given.

Finally, the reversibility of the transformation was checked. When the primary pressure is completely released down to 0.1 MPa but maintaining the sample between diamond anvils, one obtains a spectrum corresponding to that of the HP1 phase. After one day, the transformation of this spectrum into the spectrum of triclinic δ-phase is observed. After removing the sample from the gasket, the initial mixture of γ- and δ-phases is partly recovered.

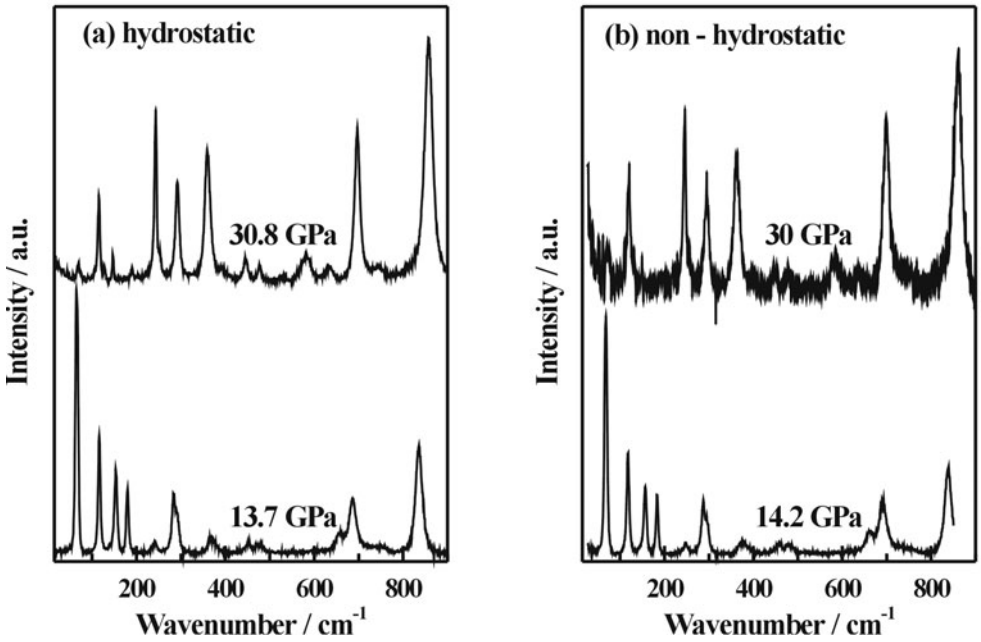

Figure 5. Raman spectra of two HP phases, HP3 and HP4, under isostatic (a) and non-isostatic (b) conditions.

5. Discussion

In the absence of a lattice dynamics calculation, only qualitative assignments of the bands, such as those proposed in table 2, can be made. However, there is no doubt that high-frequency modes involve practically pure W–O stretching motions and that the correlation lengths of these so-called hard modes are of the order of a few ångströms. Any change in their frequency is a sign that there is a structural change at short-range order. Vice versa, the low-frequency modes involve collective motions and are sensitive to long-range order—as, for instance, for librational modes of octahedra. These modes are often considered as involved in the phase transition mechanism and are expected between 30 and 200 cm^{-1}.

5.1. Structural transitions

(1) The transformation of the initial monoclinic into the triclinic form is easily achieved under non-hydrostatic conditions. The destabilization of the monoclinic phase appears to be activated by shearing strains. Thus, as stated in [11], one might suspect that this triclinic phase is stabilized by residual internal stresses and is, actually, not the stable form of WO_3 at ambient conditions. Under increasing pressure, the triclinic phase undergoes the same transformation into the HP1 phase as in the hydrostatic process reported in figure 3. The transformation is spread over a broader pressure range (apparently complete at 1.22 GPa), which is most probably due to the presence of pressure gradients revealed by some broadening of the Raman bands of the HP1 form when compared to those of figure 3. The kinetics of the transmission of pressure could also be invoked as an explanation for the delay in the complete transformation.

(2) The complete transformation into the HP1 phase is achieved above 0.1 GPa, and the important spectral changes suggest that the transition is of first order. As stated in [12],

Table 2. Raman wavenumbers of different phases. Note: bands a, b, d belong to the monoclinic γ- and triclinic δ-phases in the initial mixture. (BS stands for band symbol.)

		HP1		HP2		HP3		HP4		
Mode description	BS	$\nu_{0.36\,GPa}$ (cm^{-1})	$(\partial\nu/\partial P)_T$	$\nu_{5.37\,GPa}$ (cm^{-1})	$(\partial\nu/\partial P)_T$	$\nu_{13.7\,GPa}$ (cm^{-1})	$(\partial\nu/\partial P)_T$	$\nu_{30.1\,GPa}$ (cm^{-1})	$(\partial\nu/\partial P)_T$	BS
Octahedra	a	30.5[a]								
librations	b	44.2[a]								
W–O–W bendings	1	58.0[c]	+1.5	62.0[c]	+0.4	65.7[c]	+0.5			
	2	62.7[c]	−0.7							
	3	99.5[c]	+9.0	117.7[b]	−0.1	116.2[b]	−0.3			
								115.6[b]	+0.6	A
	4	100.1[c]	+9.1	144.3[b]	+1.8	153.4[b]	+0.9			
								128.5[a]	+1.3	B
								147.1[a]	+0.2	C
	5	143.8[b]	+7.1	164.1[b]	+2.5	179.9[b]	+1.6			
	1			172.1[a]	+0.2					
	6	182.0[b]	+3.7	204.3[b]	+4.8	241.2[a]	+4.1			
	7	198.2[b]	−3.5							
								243.2[b]	+0.7	D
								253.8[a]	+0.2	E
O–W–O bendings	8	268.4[b]	+2.1	276.2[b]	+0.9	283.8[b]	+1.1			
								292.2[b]	+0.7	F
	2			280.1[a]	+1.4	292.4[a]	+1.6			
	9	309.6[b]	+5.5	324.9[b]	+5.6					
	9a					369.0[a]	+2.5			
	9b					372.0[a]	+3.8			
								360.1[c]	+1.1	G
	10	379.6[a]	+9.2	419.0[a]	+4.58	451.8[a]	+3.7			
								445.9[a]	+1.1	H
								477.4[a]	+0.6	I
	11	426.2[a]	+5.5	446.0	+3.5	471.3[a]	+3.2			
	12			459.1	+3.5	482.0[a]	+3.0			
								528.2[a]	+4.3	J
								581.9[a]	+2.3	K
								633.2[a]	+1.5	L
W–O stretching	13	636.4[b]	+1.9	640.2[b]	+1.8	657.0[a]	+2.6			
	14	673.1[b]	0.0	672.8[b]	+1.3	686.4[b]	+1.9			
								697.0[c]	+1.6	M
	d	703.8[a]	−4.0							
								745.0[a]	+1.8	N
	15	734.5[a]	−4.1	731.3[a]	+1.5	745.5[a]	+2.0			
	16	809.4[c]	+3.7	822.2[c]	+1.7	835.6[c]	+1.8			
								858.2[c]	+0.3	O

[a] Weak.
[b] Medium.
[c] Strong.

the sample could be in the same phase as that obtained with a single crystal above 1.01 GPa by Xu *et al* [8] and described by the space group $P2_1/c$ ($Z = 4$) from an XRD study. However, this HP1 phase, as observed from Laue photographs up to 0.5 GPa, is attributed to the monoclinic ε-form in [11] with space group Pc ($Z = 4$). From their Raman investigation, Souza-Filho *et al* [12] report that the high-pressure HP1 form is the ε-form

but conclude that this form is described by space group $P2_1/c$ ($Z = 4$) in disagreement with the original space group of [11]. Actually, the ε-phase is a form which was previously obtained at low temperature and whose Raman spectrum is somewhat different [16] from that discussed above. However, the possible $P2_1/c$ and Pc structures for WO_3 in its HP1 form cannot be easily discriminated from diffraction data obtained on a polycrystalline sample [17]. In this phase, 21 Raman modes are observed, and this favours the $P2_1/c$ space group for which 24 modes are expected rather than 45 as for the Pc group. The replacement of the band at 715 cm^{-1} in the initial spectrum, noted in figure 1, and observed between 10 MPa and 0.018 GPa (this pressure range is too small to be clearly represented in figure 4) as the 636–673 cm^{-1} doublet, suggests that some W–O bonds become longer and that the octahedra are more distorted in this form. This interpretation is in agreement with the values of W–O distances given in [8]. The longest bonds become even longer at the phase change, while the shortest ones become even shorter.

Souza-Filho *et al* [12] on the one hand and Xu *et al* [8] on the other hand have concluded that this phase was stable up to 5 GPa, the maximum pressure in their investigations. As a matter of fact, the general aspect of the spectra is retained up to 22 GPa, and it is tempting to conclude that the phase HP1 is stable up to this pressure. However, considering now the $\nu = f(P)$ plots represented in figure 4, it is possible to identify spectral changes; i.e. the derivatives of $\nu = f(P)$ plots of several bands change from a finite value to nearly zero at about 3 and 10 GPa. These anomalies as well as the softening of modes 7–15 between 0.1 and 3 GPa or 3 between 5 and 22 GPa under increasing pressure reveal that the distributions of anharmonic couplings between the different normal modes change with pressure, and this might indicate that Raman-inactive modes are involved in a structural transition mechanism.

(3) Above 3 GPa, the small spectral changes of figure 4 make it difficult to ascertain the occurrence of a new phase. However, the corresponding changes in the dynamics of the sample are an indication that a slight structural change has taken place at about 3 GPa and that up to 10 GPa the spectral parameters exhibit a quasi-linear pressure dependence and do not present any anomaly. This structural state is labelled HP2 in the following.

(4) Above 10 GPa, except the subtle changes already mentioned, the spectra are quite close to those obtained for HP2 and, thus, the structure HP3 of the sample must still be quite close to that described for HP2.

(5) The drastic spectral changes observed at about 22 GPa suggest that the associated transition is of first order. Persistent HP3 bands can be related to the fact that the local pressure remains constant throughout the transformation of this phase, which is a clear indication that the sample has not completely achieved its transformation. The existence of a pressure gradient at such high pressures can explain why some parts of the sample are already in the HP3 phase while others are still transforming; it is for the latter parts that the local pressure is fixed. The spectra of the HP4 phase, although quite different from those of the low-pressure phases, contain at least 15 bands, and the corresponding structure can probably be described with the same cell multiplicity as HP1, 2, 3; a low symmetry with pronounced atomic displacements might be considered.

5.2. Effect of the pressure-transmitting medium

Surprisingly, the non-hydrostatic conditions do not induce inhomogeneous band broadening. Figure 5 shows that the spectra obtained without alcohol are remarkably similar to those obtained with alcohol, as if the sample was isotropic by itself in its low-pressure and HP phases. To the best of our knowledge, this is a rare example where the anisotropy of the

applied pressure does not induce a substantial broadening of the bands. Furthermore, the non-hydrostatic conditions do not alter the phase transition sequence observed in hydrostatic conditions. In fact, the strong reduction of intensity of the HP4 spectrum, when obtained without alcohol, is the only notable difference. This sudden loss of intensity beyond 22 GPa is due to strong absorption and/or reflection losses, which might be related to a strong gap reduction. A similar observation was reported for nanocrystalline WO_3 [2]. In any case, no traces of amorphization are evident in the non-hydrostatic HP spectra. den Wijs *et al* [13] in their first-principles calculations were led to conclude that the gap widens upon pressure; however, that study was limited to a narrow range of pressure and it is probable that the structural trends reported for pressures below 5 GPa are quite different above 25 GPa.

5.3. Compressibilities

5.3.1. The Hazen model. The Hazen model [18] is based on nearest-neighbour interactions, which are considered to be responsible for the crystal structure and properties. It assumes that thermoelastic properties of a crystal are dominated by the individual properties of cation polyhedra. Thus the volume compressibility coefficient for an oxide, based on a polyhedron assemblage, is given by

$$\kappa = (S/Z_{anion})(d^3/Z_{cation}) \times 10^{-11}\ \mathrm{Pa}^{-1} \tag{1}$$

where d is the average distance in Å between the cation and anion and Z is the cation or anion charge. S is an adjustable parameter taking into account the ionic or covalent character of the crystal. For ionic oxides, the S/Z_{anion} factor is equal to 0.133. Taking into account that WO_6 octahedra are distorted and W–O distances vary from 1.78 to 2.14 Å [8] in the 0.01–4.5 GPa range, one obtains an average compressibility equal to 1.6×10^{-12} Pa^{-1}, or bulk modulus B_H (defined as $B_0 = \kappa^{-1}$) equal to 625 GPa. Such a value—much larger even than that for diamond (about 400 GPa)—is unrealistic. Such a discrepancy between calculated and observed compressibilities is unusual for ABO_3 perovskites; it probably arises because the large O_{12} polyhedral cavity is occupied by a cation A, the electrons of which (via oxygen–electron repulsions) contribute to a decrease in the compressibility. In usual perovskites, the cell compressibility might be obtained by adding the polyhedra compressibilities weighted by the corresponding volumes following the relationship proposed in [19]:

$$\kappa_{cell} = \frac{\kappa_o V_o + \kappa_p V_p}{V_{cell}}. \tag{2}$$

In a cubic perovskite the volume ratios are equal to 1/6 for octahedra and 5/6 for AO_{12} polyhedra [19, 20].

A similar situation can be achieved in WO_3, by decreasing the formal charge of W from 6^+ to $(6-q)^+$ and placing a virtual cation of charge q in the centre of the cation-free O_{12} polyhedron. Since the advent of quantum mechanics, one has had to be prepared to accept that there is a non-zero electronic density originating from the surrounding ligands, even in the unoccupied cation site, and that an empty polyhedron can participate in the compressibility. With $q = 2$, one can easily force the compressibility to have a reasonable order of magnitude. For instance, to retrieve the value of the bulk modulus published in [8]: $B_0 = 44.5$ or 25 GPa, one must consider that 26 or 14% respectively of the positive tungsten charge is transferred in the O_{12} polyhedron site. Such a change cannot be obtained by simply adjusting the 'ionicity' S-parameter. Thus, in order to obtain reasonable compressibilities, in the case of non-compact structures, rather than performing a summation of inverse compressibilities of polyhedra as in [21], it seems preferable to extend the Hazen model as above. One can find some justification for assuming charge delocalization, as invoked above, from considering the band structure of

this type of oxide. Strongly dispersive crystalline orbitals in this compound are calculated, an indication of a high mobility of electrons, i.e. leading to a compound which is not purely ionic. Significant covalent effects for non-cubic phases of WO_3 are underlined in [13].

5.3.2. Volume compressibilities deduced from Raman results. The pressure dependence of the frequency of a normal mode is related to the compressibility of the crystal and to the so-called isothermal Grüneisen parameter γ defined by

$$\gamma = \frac{1}{\kappa}\left(\frac{\partial \ln \nu}{\partial P}\right)_T. \tag{3}$$

A γ_i-parameter is thus defined for each normal mode of frequency ν_i. This parameter, which gives the normalized (to volume variation) pressure dependence of a mode, is a measure of the temperature-independent anharmonicity of the mode [19].

Under the condition of invariance of κ in the range of the volume variation considered, the integration of (3) gives

$$\nu = \nu_0 e^{\gamma\kappa(P-P_0)}. \tag{4}$$

This relationship shows that the $\nu = f(P)$ plots should be exponential curves with a positive concavity and that any deviation from this behaviour is an indication of some crystal instability and that the anharmonicity becomes important.

For small values of the exponent, one can limit the development of the exponential to the first linear term and one finds

$$\gamma\kappa = (1/\nu_0)\partial\nu/\partial P. \tag{5}$$

This term is designated by K and is also called the pressure coefficient of the corresponding mode. The derivatives of the $\nu = f(P)$ plots for each mode are reported in table 2 for four selected pressures:

(i) 0.36 GPa is chosen in the middle of the existence domain of the HP1 phase;
(ii) 5.37 GPa, in contrast, is close to the pressure range in which strong spectral variations take place;
(iii) 13.7 GPa corresponds to a linear variation of all the wavenumbers and can be representative of the sample in a quasi-harmonic state still far from its HP4 structure;
(iv) the highest pressure is representative of the completely transformed sample.

The relationship between γ and κ can be described with the polyhedral model as developed recently for perovskites [19] in the quasi-harmonic and in the cubic approximations. The volume compressibility of a polyhedron can be written as

$$\kappa = \frac{6}{m+n+3}K \tag{6}$$

where m and n are exponents related to attractive and repulsive atom–atom potentials, respectively [22]. Comparison between equations (5) and (6) shows that the factor in front of K is the reciprocal of γ. For ionic crystals, $m = 9$ and $n = 1$. This result is equivalent to considering that $\gamma = 13/6$ for the modes involving the bond stretching of a polyhedron and that $\kappa = 0.461$ K. In covalent crystals, $m + n$ lowers to three [22, 23] and $\kappa = K$. Thus by taking into account equations (5) and (6) and the relative volume of a polyhedron, the compressibility of a polyhedron is given by

$$\kappa = \frac{6}{m+n+3}\frac{1}{\nu_0}\left(\frac{\partial\nu}{\partial P}\right)\frac{V}{V_{cell}}. \tag{7}$$

In the HP1 phase, among the four bands due to the W–O high-frequency stretching modes, three exhibit zero or an important negative slope (-4.1 for mode 15). The average slope is

about -3 ($K = -3/700$ GPa^{-1}) and it can be concluded that octahedra 'prefer' to undergo W–O bond expansion below 10 GPa before exhibiting a positive compressibility. In contrast, the low-frequency modes involving W–O–W bendings (equivalent to octahedra librations and translations), and thus able to deform the empty O_{12} polyhedra, exhibit exceptionally large derivatives (+9.0 for mode 3, +7 for mode 5, +9.1 for mode 4). This is an indication that the O_{12} polyhedra are highly deformable and are responsible for the small bulk modulus of the sample below 5 GPa.

In the absence of any result from normal-mode calculation, the choice of the appropriate modes is difficult. However, if one considers that the most sensitive mode, mode 4 at 102 cm^{-1}, in table 2 is a mode involving the deformation of the O_{12} polyhedron, the application of equation (7) to the estimation of the compressibility of a polyhedron of volume $(5/6)V_{cell}$ gives $\kappa_{polyhedron} = 0.461 \times 9.1 \times 1/102$ GPa^{-1} $= 4.113 \times 10^{-11}$ Pa^{-1} in the case of a pure ionic model and 7.43×10^{-11} Pa^{-1} in the case of a pure covalent model.

In the same way, considering the highest mode, mode 16, for the octahedra deformation, one gets $\kappa_{octahedra} = 0.461 \times 3.7 \times 1/809$ GPa^{-1} $= 0.21 \times 10^{-11}$ Pa^{-1}, and the cell compressibility is found to be determined mainly by the O_{12} polyhedron. By volume weighting these compressibilities (by 5/6 and 1/6 respectively) one obtains the cell compressibility, the inverse of which for the HP1 phase gives a bulk modulus lying between 28.9 and 16.1 GPa for the ionic and covalent cases respectively. The ionic value is of the same order of magnitude as that reported by Xu *et al* (44 GPa) and that (25 GPa) found in our recent XRD study [17]. One must be aware that none of these values can be considered as sound. In principle, x-ray data should be the most reliable; however, in the present case, because the pressure range below the first transition (below 0.1 MPa) is small, the measurement of the relative changes of the unit-cell volume are not precise and in any case the derivation of the bulk modulus of WO_3 from data up to 5 GPa, as carried out in [8], overestimates this modulus. In the same way, the derivation of the compressibility from spectroscopic data is only indicative. In any case, by taking into account the covalent character of the sample, it is possible to make adjustment: for example, taking $m + n = 8.1$ instead of 10 as for the purely ionic case allows one to obtain a bulk modulus of 25 GPa as found from our recent crystallographic observations. In such cases, one could propose that the ionicity is lowered by 20%.

It is readily seen that the same calculation made with the data of table 2 ($\nu = 153$ cm^{-1} and $\mathrm{d}\nu/\mathrm{d}P = 0.9$ cm^{-1} GPa^{-1}) for the HP3 phase leads to a bulk modulus nearly ten times larger. A similar order of magnitude is obtained for the HP4 phase when using the average parameters of the low-frequency modes A, B, C. One should note that the cubic approximation certainly becomes less and less appropriate for high pressures, and that the volume of octahedra relative to that of O_{12} polyhedra might become far from 1/5. As a consequence, the tungsten oxide appears as a soft material at ambient conditions and becomes very hard at high pressure. Notice that qualitative conclusions on the relative mechanical properties of HP1 and HP4 phases can be obtained from a simple examination of the frequency plots. For the HP4 phase, all the $\nu = f(P)$ plots are linear and present a small slope, while the situation is the reverse for HP1. This is an indication that the HP4 phase is far from a transition and is less compressible than the low-pressure phase.

These conclusions remain qualitative, but give insight into the properties of this material and of the perovskite compounds. It can be concluded that in perovskites the BO_6 octahedra are rigid entities, which determine the structure but do not contribute much to the total compressibility because of their small (1/6) relative volume. In contrast, the O_{12} polyhedra are more deformable entities and, because of their relatively large volume (5/6), they dominate in the overall summation of individual compressibilities. In the absence of the A cation, a softening of the material is observed. This is in agreement with the fact that the low-frequency

modes, representing deformations of the O_{12} polyhedra, are downshifted in WO_3 compared to perovskites, and that this leads to a decrease in the bulk modulus. Thus low-frequency modes, like the bulk modulus, appear as mainly governed by electron–electron repulsions taking place in polyhedra. The hardening of WO_3 at high pressure is probably due to a strong structural change accompanied by an increase of the electronic density in the O_{12} polyhedra, either due to a shortening of the O–O distances or to an increase of the charge transfer associated with the appearance of a strong absorbance for the high-pressure phase. Finally, one may suggest that the concept of electronic density in polyhedra would provide a more convenient parameter than the cation charge, as it appears in Hazen's expression for compressibility. In fact, Z_{cation}/d^3 appears as a mirror of the electronic density associated with anions surrounding the cation or the virtual cation. The advantage of considering electronic density is that it can be taken into account for polyhedra in which the central cationic site is vacant. This model might explain the increase of the bulk modulus with the increase of the electronic density. In ReO_3, the rhenium is in a $5d^1$ configuration and gives its extra electron to the conduction band (antibonding states made of oxygen 2p and metal 5d orbitals). This might explain why the bulk modulus increases from 25 GPa for WO_3 to 100 GPa for ReO_3 in its cubic phase [24].

6. Conclusions

A Raman HP study has been performed on pure microcrystallized tungsten oxide up to 31 GPa in a DAC. Our study confirms the phase transition taking place at about 0.1 GPa, already reported in the literature, while a new HP phase labelled HP4 is obtained at 22 GPa. These two latter transitions are characterized by marked spectral discontinuities and are most probably of first order. The octahedra are strongly distorted, as can be concluded from the broad frequency range in which W–O stretching modes are observed. Spectral derivative discontinuities, which are observed near 3 and 10 GPa, might correspond to small structural changes without necessarily involving a change of space group. Surprisingly, the non-hydrostatic conditions do not induce inhomogeneous band broadenings and do not modify the transition sequence observed in hydrostatic conditions. Grüneisen parameters and compressibilities have been derived from the pressure dependences of the modes involving specifically stretching motions of individual O_{12} polyhedra of the structure. The total compressibility is written as a summation of individual volume-weighted polyhedra compressibilities. Polyhedra compressibilities were estimated from the pressure dependence and a reasonable agreement between the bulk modulus value derived from this model and that found from x-ray experiments is obtained. The compressibility of the crystal was also derived by using the Hazen model. To obtain the right order of magnitude, we propose an extension of this model consisting of the introduction of an adjustable hole transfer in the unoccupied O_{12} polyhedron.

Acknowledgment

Jens Kreisel is acknowledged for discussion and a critical reading of the manuscript.

References

[1] Bouvier P and Lucazeau G 2000 *J. Phys. Chem. Solids* **61** 569–78
[2] Boulova M, Lucazeau G, Pagnier T and Gaskov A 2000 *Proc. ICORS 2000: 17th Int. Conf. on Raman Spectroscopy* pp 166–7
[3] Pagnier T, Boulova M, Galerie A, Gaskov A and Lucazeau G 1999 *J. Solid State Chem.* **143** 86–94
[4] Pagnier T, Boulova M, Galerie A, Gaskov A and Lucazeau G 2000 *Sensors Actuators* B **71** 134–9

[5] Howard C, Luca V and Knight K 2002 *J. Phys.: Condens. Matter* **14** 377–87
[6] Salje E 1975 *Acta Crystallogr.* A **31** 360–3
[7] Salje E and Viswanathan K 1975 *Acta Crystallogr.* A **31** 356–9
[8] Xu Y, Carlson S and Norrestam R 1997 *J. Solid State Chem.* **132** 123–30
[9] Hayashi S, Sugano H, Arai H and Yamamoto K 1992 *J. Phys. Soc. Japan* **61** 916–23
[10] Souza-Filho A G, Freire V N, Sasaki J M, Filho J M, Juliao J F and Gomes U U 2000 *J. Raman Spectrosc.* **31** 451–4
[11] Salje E and Hoppmann G 1980 *High Temp.–High Pressures* **12** 213–16
[12] Souza-Filho A G, Freire V N, Pilla O, Ayala A P, Filho J M, Melo F E A, Freire V N and Lemos V 2000 *Phys. Rev.* B **62** 3699–703
[13] den Wijs G A, de Boer P K, de Groot R A and Kresse G 1999 *Phys. Rev.* B **59** 2684–93
[14] MacGillavry C H and Rieck G D 1962 *International Tables for X-ray Crystallography* vol 3 (Birmingham: Kynoch) p 318
[15] Priermarini G J, Block S, Barnett J D and Forman R A 1975 *J. Appl. Phys.* **46** 2774
[16] Boulova M and Lucazeau G 2002 *J. Solid State Chem.* at press
[17] Bouvier P, Crichton W, Boulova M and Lucazeau G 2001 *J. Phys.: Condens. Matter* submitted
[18] Hazen R M 1985 *Rev. Mineral.* **14** 324
[19] Loridant S and Lucazeau G 1999 *J. Raman Spectrosc.* **30** 485–92
[20] Chemarin C, Rosman N, Pagnier T and Lucazeau G 2000 *J. Solid State Chem.* **149** 298–307
[21] Kreisel J and Glazer A M 2000 *J. Phys.: Condens. Matter* **12** 9689–98
[22] Sherman W F and Wilkinson G R 1980 *Advances in Infrared and Raman Spectroscopy* (London: Heyden) ch 4, p 232
[23] Mougin J, Bihan T L and Lucazeau G 2001 *J. Phys. Chem. Solids* **62** 553–63
[24] Jorgensen J E, Olsen J S and Gerwarg L 2000 *J. Appl. Crystallogr.* **33** 279